Electronic Supplementary Information (ESI) for

Surface-functionalized three-dimensional MXene supports to boost hydrogen evolution activity of Pt catalysts in alkaline media

Haeji Hong,[ab†] Ho Young Kim,[c†] Won Il Cho,[d] Ho Chang Song,[e] Hyung Chul Ham,[e] Kyunghee Chae,[f] Filipe Marques Mota,*[fg] Jin Young Kim*[c] and Dong Ha Kim*[fhi]

[a] Department of Chemical Engineering and Materials Science, College of Engineering, Ewha Womans University, 52, Ewhayeodae-gil, Seodaemun-gu, Seoul 03760, Republic of Korea.

[b] Graduate Program in System Health Science and Engineering, Ewha Womans University, 52, Ewhayeodae-gil, Seodaemun-gu, Seoul 03760, Republic of Korea.

[c] Center for Hydrogen·Fuel Cell Research, Korea Institute of Science and Technology (KIST), Seoul 02792, Republic of Korea.

[d] Center for Energy Storage Research, Korea Institute of Science and Technology (KIST), Seoul 02792, Republic of Korea.

[e] Department of Chemical Engineering, Inha University, Inha-ro 100, Michuhol-gu, Incheon 22212, Republic of Korea.

[f] Department of Chemistry and Nano Science, Division of Molecular and Life Sciences, College of Natural Sciences, Ewha Womans University, 52, Ewhayeodae-gil, Seodaemun-gu, Seoul 03760, Republic of Korea.

[g] School of Chemistry, University of Lincoln, Brayford Pool, Lincoln, Lincolnshire LN6 7TS, United Kingdom

[h] Basic Sciences Research Institute (Priority Research Institute), Ewha Womans University, 52, Ewhayeodae-gil, Seodaemun-gu, Seoul 03760, Republic of Korea.

[i] Nanobio·Energy Materials Center (National Research Facilities and Equipment Center), Ewha Womans University, 52, Ewhayeodae-gil, Seodaemun-gu, Seoul 03760, Republic of Korea.

[†]These authors contributed equally to this work.

Characterization

The surface morphology of the MXene was revealed in a JEOL JSM6700-F scanning electron microscope (SEM), in a JSM-7610F high-resolution SEM (HR-SEM), and in a JEM-2100Plus transmission electron microscopy (TEM). Raman spectroscopy (LabRam HERvo 800) was used within a 100 to 1900 cm^{-1} range for the optical measurement of MXene. The crystallinity, structure, and terminations of the samples were investigated by X-ray diffractometer (D/MAX-2200/VPC) and Fourier-transform infrared Spectrometer (INVENIO-R). To differentiate specific terminations on the MXene surface, X-ray photoelectron spectroscopy (XPS) was performed on a Thermo Scientific K-Alpha XPS with a dual beam source and ultra-low energy electron beam. The surface area of all nanostructures was investigated by an ASAP 2020 Micromeritics instrument.

Computational details

All calculations were carried out on the basis of spin-polarized density functional theory (DFT) as implemented in the Vienna Ab-initio Simulation Package (VASP).[S1] The projector augmented wave (PAW) method using a plane wave basis set was implemented to describe the interaction between core and valence electrons.[S2] The Perdew–Burke–Ernzerhof (PBE) exchange–correlation functional within a generalized gradient approximation (GGA) was employed.[S3, S4] An energy cutoff of 400 eV was used for the plane wave expansion of the electronic eigenfunctions.

To model the $Ti_3C_2T_x$ [T=–F, –O, –OH] surfaces, we expanded the Ti_3C_2 bulk unit cell having a P63/mmc structure with the different surface terminations i.e., –F, –O and –OH functional groups, and set the vacuum space in the z-direction to at least 15Å to prevent the interaction between periodic images. The pyramid-like Pt_4 cluster is located on the surface of $Ti_3C_2T_x$ [T=–F, –O, –OH] slabs for simulating the Pt catalyst supported on $Ti_3C_2T_x$ [T=–F, –O, –OH]. All the atoms were fully relaxed using the conjugate gradient method until residual forces on all the constituent atoms became smaller than 5×10^{-2} eV/Å. For the Brillouin zone integration, we accepted (10×10×10) and (5×5×1) Monkhorst-Pack mesh of k-points to determine the equilibrium geometries and total energies of bulk Ti_3C_2 and $Ti_3C_2T_x$, respectively.[S5]

To calculate free energy of the electrocatalytic HER (hydrogen evolution reaction), we followed J. K. Nørskov's procedures using Equation (1):[S6]

$$\Delta G = \Delta E - T\Delta S + \Delta ZPE - neU \qquad (1)$$

Where ΔE is the total energy at $T=0$ K, ZPE is the zero potential energy, ΔS and T are the change of entropy and the temperature at $T=298.15$ K. Here, n and U are the number of electron transfer during reaction, and the operating electrochemical potential over standard hydrogen electrode. The vibrational entropy of the adsorbed species was obtained from frequency calculation, and the entropy of gaseous molecules under reaction conditions were taken from the NIST Chemistry WebBook.[S7]

Supplementary data

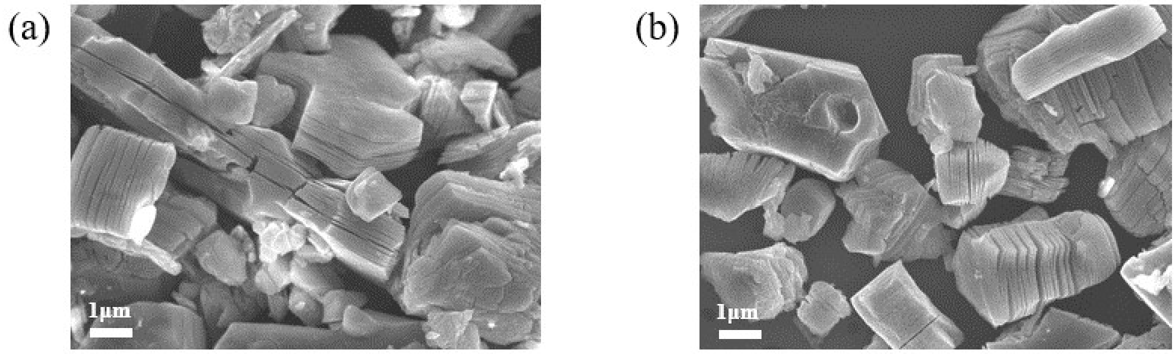

Fig. S1 Supplementary characterization of etched $Ti_3C_2T_x$. SEM images of etched $Ti_3C_2T_x$ in HF (~50%) solution for (a) 1 day and (b) 2 days.

Table S1 Inductively Coupled Plasma (ICP) result of Ti_3AlC_2 and Ti_3C_2 after HF treatment for 3 days.

Sample	Concentration (Ti)	RSD (%)	Concentration (Al)	RSD (%)	Ti/Al ratio
Ti_3AlC_2	65.117	0.19	7.933	0.16	4.63
Ti_3C_2 (48% HF, 3 days)	88.846	0.14	2.588	0.72	19.34

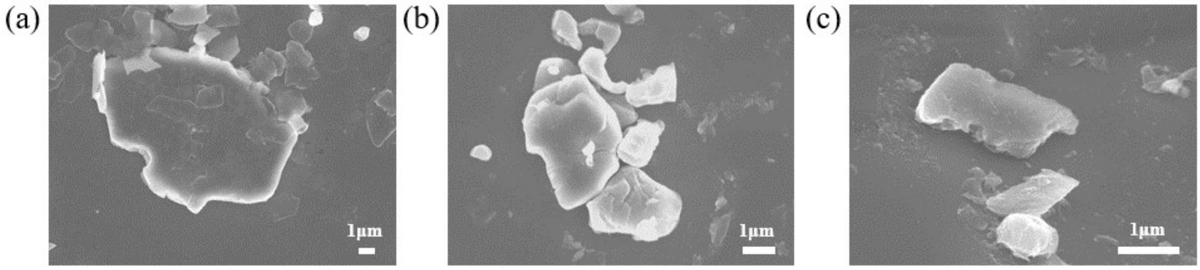

Fig. S2 Supplementary characterization of the exfoliated $Ti_3C_2T_x$. The collected SEM images showcase the presence of remaining bulk $Ti_3C_2T_x$ following tip-sonication carried out for (a) 1 h, (b) 2 h, and (c) 3 h.

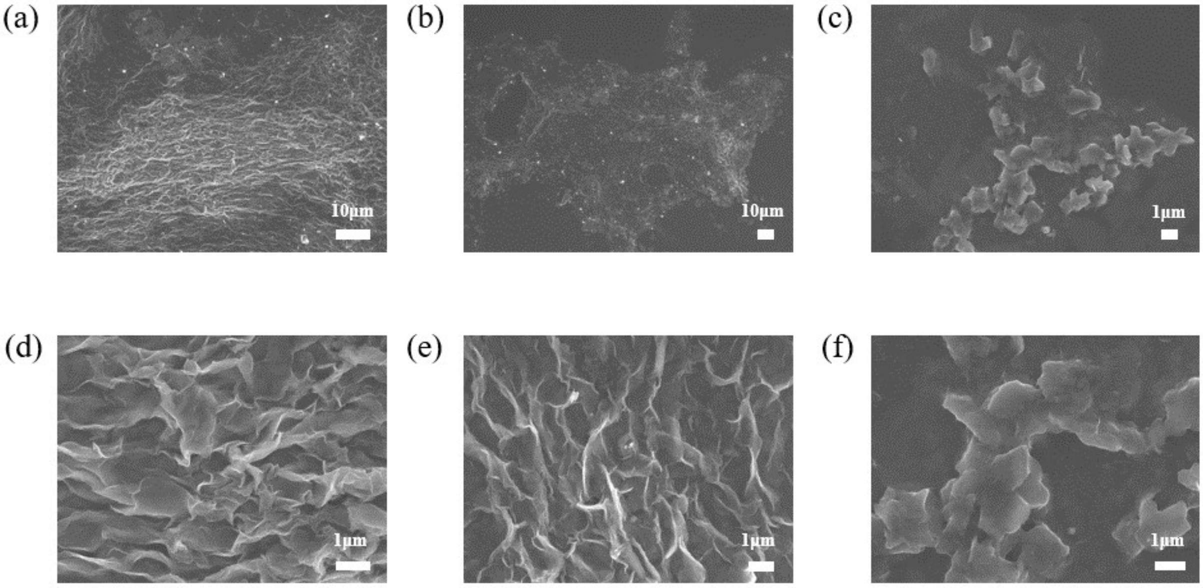

Fig. S3 Supplementary images of alkali-induced 3D MXene with different alkali solutions. SEM images of 3D $Ti_3C_2(OH)_x$ samples in (a, d) NaOH solution, (b, e) KOH solution, and (c, f) LiOH solution.

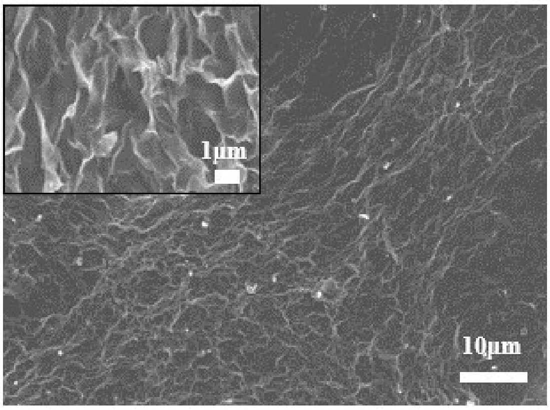

Fig. S4 Supplementary SEM images of the alkali-induced 3D $Ti_3C_2(OH)_x$ MXene treated with increasing concentration of the NaOH solution (2 M). Inset is the high-resolution SEM image.

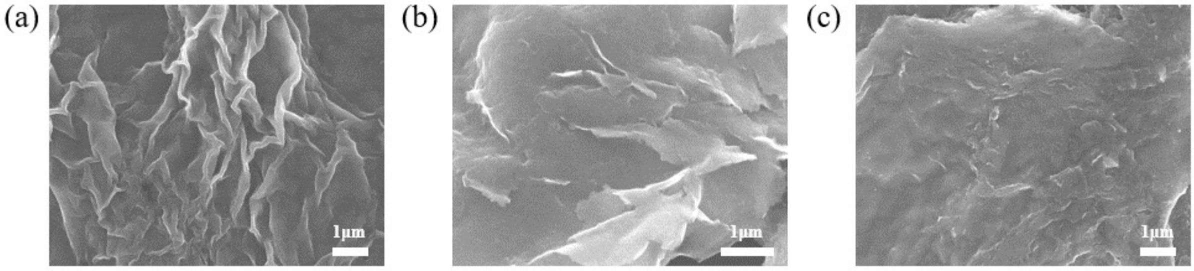

Fig. S5 Supplementary images of alkali-induced 3D MXene with HF (~50%) under increasing treatment times. SEM images of 3D $Ti_3C_2F_x$ after reacting with HF for (a) 30 min, (b) 1 h, and (c) 2 h.

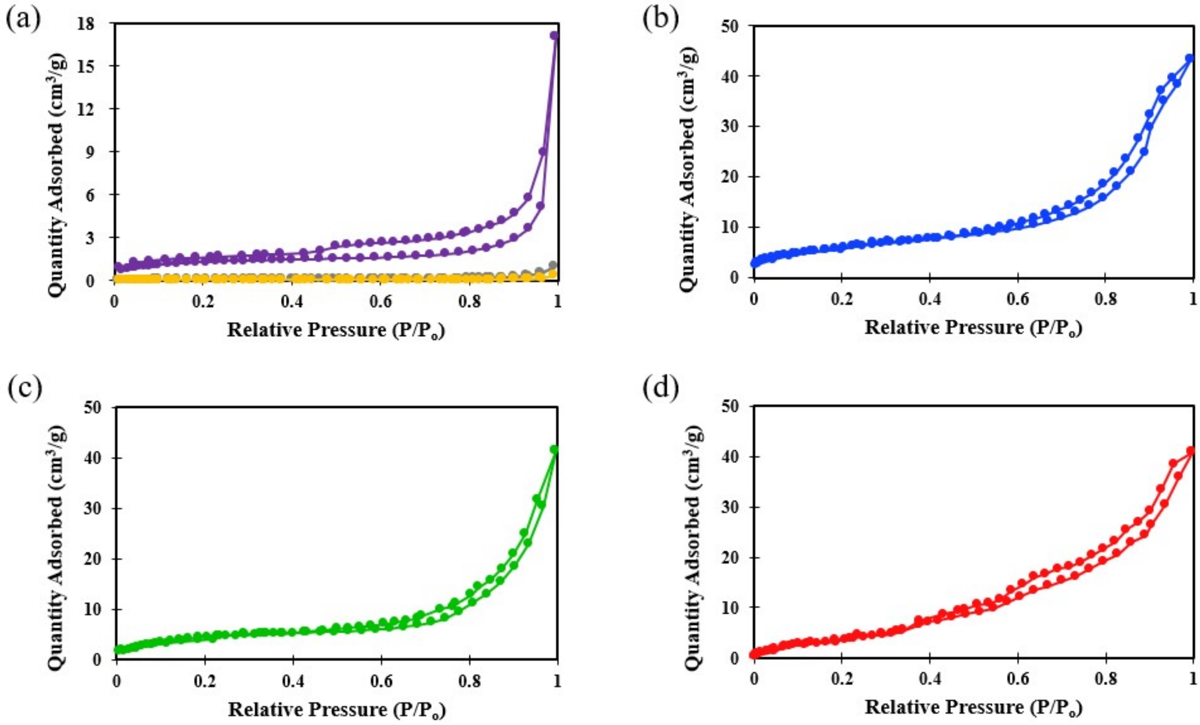

Fig. S6 Nitrogen adsorption-desorption isotherms of (a) Ti_3AlC_2 MAX (yellow), etched Ti_3C_2 (gray), and exfoliated 2D Ti_3C_2 (purple), (b) 3D $Ti_3C_2(OH)_x$, (c) 3D $Ti_3C_2O_x$, and (d) 3D $Ti_3C_2F_x$.

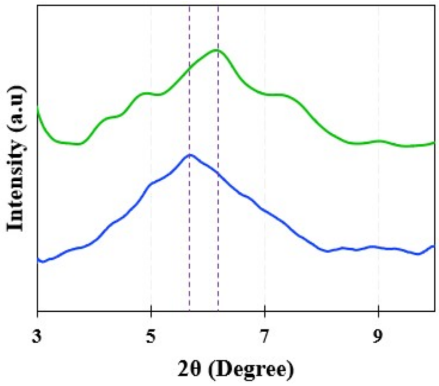

Fig. S7 Magnified XRD spectra of $Ti_3C_2(OH)_x$ (blue) and $Ti_3C_2O_x$ (green).

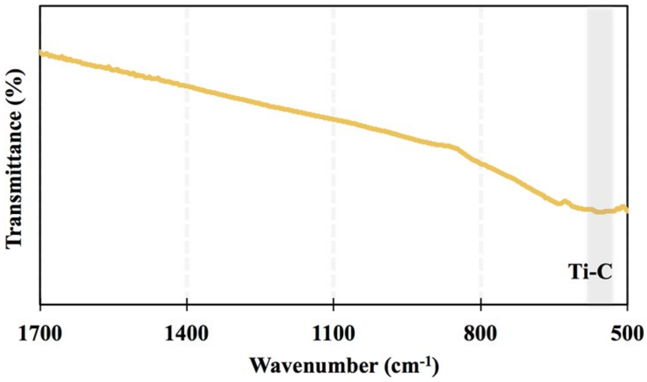

Fig. S8 FT-IR spectra of etched Ti_3C_2.

Table S2 Contents of each termination groups in each MXene sample, as determined by the deconvolution and integration of corresponding areas from the XPS results.

Sample	–OH	–O	–F
$Ti_3C_2(OH)_x$	**51.5 %**	24.0 %	24.5 %
$Ti_3C_2O_x$	37.6 %	**55.8 %**	6.5 %
$Ti_3C_2F_x$	21.1%	19.7 %	**59.2 %**

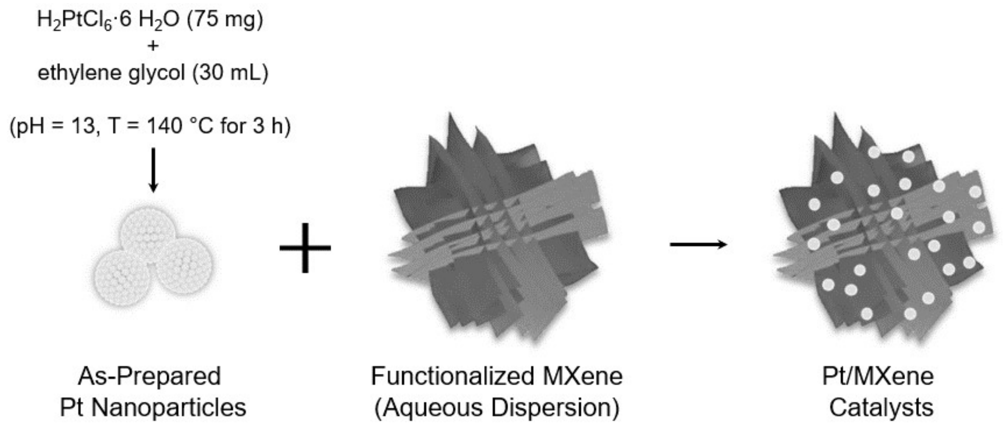

Fig. S9 Synthetic scheme of loading Pt NPs on functionalized MXene.

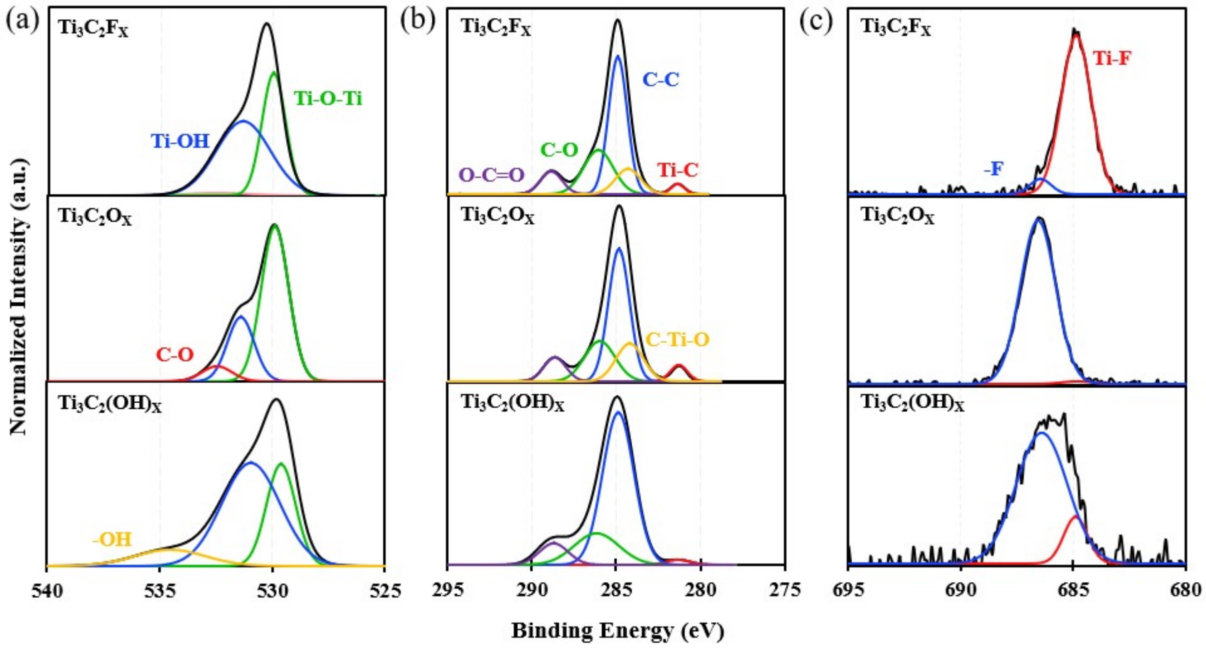

Fig. S10 (a) O 1s, (b) C 1s, and (c) F 1s XPS spectra for Pt/$Ti_3C_2T_x$ (T=–OH, –O, and –F).

Table S3 Contents of each termination groups in each Pt-loaded MXene sample, as determined by the deconvolution and integration of corresponding areas from the XPS results.

Sample	–OH	–O	–F
$Ti_3C_2(OH)_x$	**57.5 %**	28.5 %	14.0 %
$Ti_3C_2O_x$	28.4 %	**70.0 %**	1.5 %
$Ti_3C_2F_x$	29.7 %	21.3 %	**49.0 %**

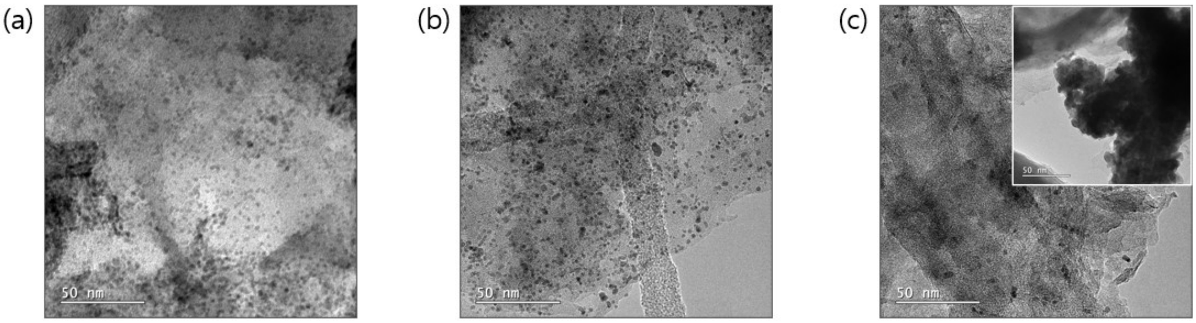

Fig. S11 TEM images of (a) 3D $Ti_3C_2(OH)_x$, (b) 3D $Ti_3C_2O_x$, and (c) 3D $Ti_3C_2F_x$; Inset is TEM image of aggregated Pt NPs on 3D $Ti_3C_2F_x$.

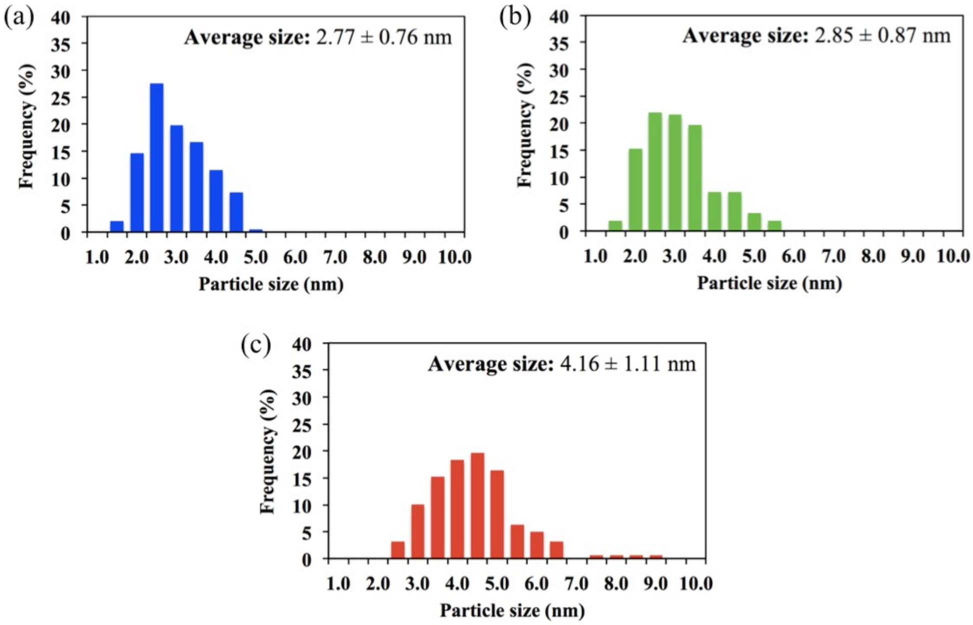

Fig. S12 Pt particle size distribution (<10 nm) and corresponding average sizes over (a) $Pt/Ti_3C_2(OH)_x$, (b) $Pt/Ti_3C_2O_x$, and (c) $Pt/Ti_3C_2F_x$.

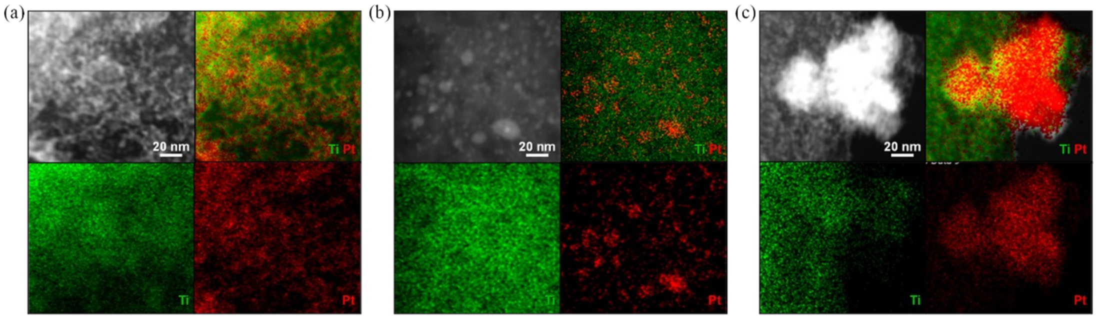

Fig. S13 EDS mapping images for (a) 20 wt.% Pt/$Ti_3C_2(OH)_x$, (a) 20 wt.% Pt/$Ti_3C_2O_x$, and (c) 20 wt.% Pt/$Ti_3C_2F_x$.

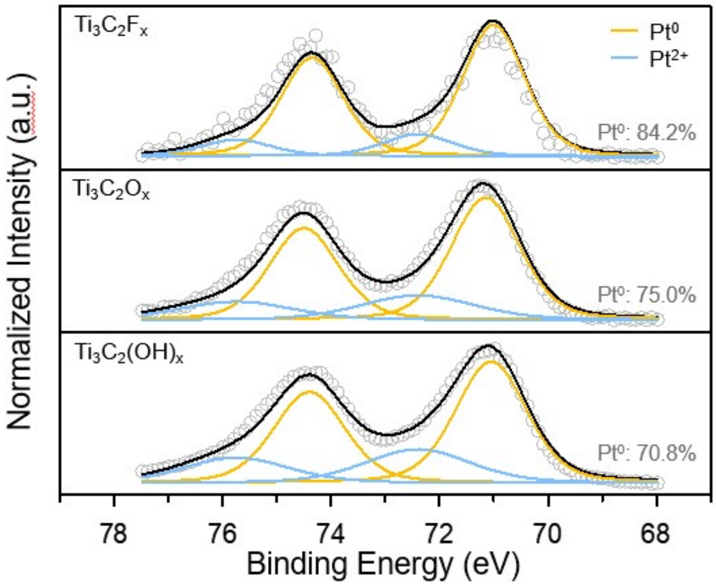

Fig. S14 Pt 4f XPS spectra for Pt/$Ti_3C_2T_x$ (T = –OH, –O, and –F).

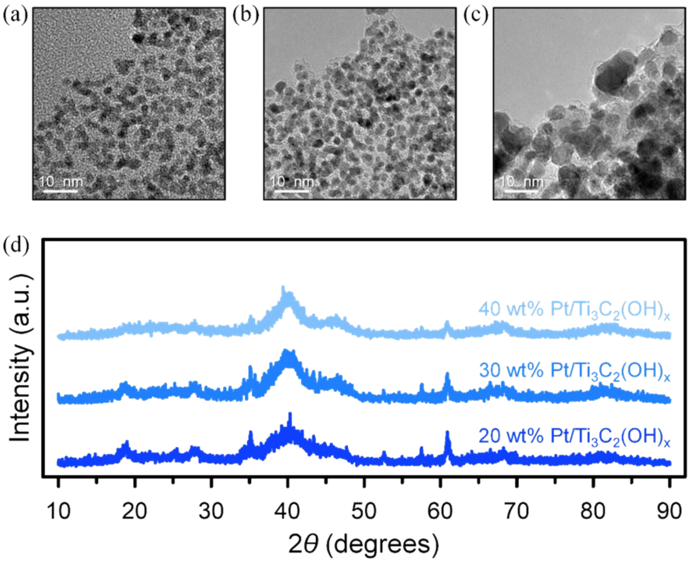

Fig. S15 Physicochemical characterization of Pt/$Ti_3C_2(OH)_x$ samples with different Pt loading. (a–c) TEM images of (a) 20 wt.%, (b) 30 wt.%, (c) 40 wt.% Pt/$Ti_3C_2(OH)_x$ samples. (d) XRD patterns of Pt/$Ti_3C_2(OH)_x$ samples with different Pt loading.

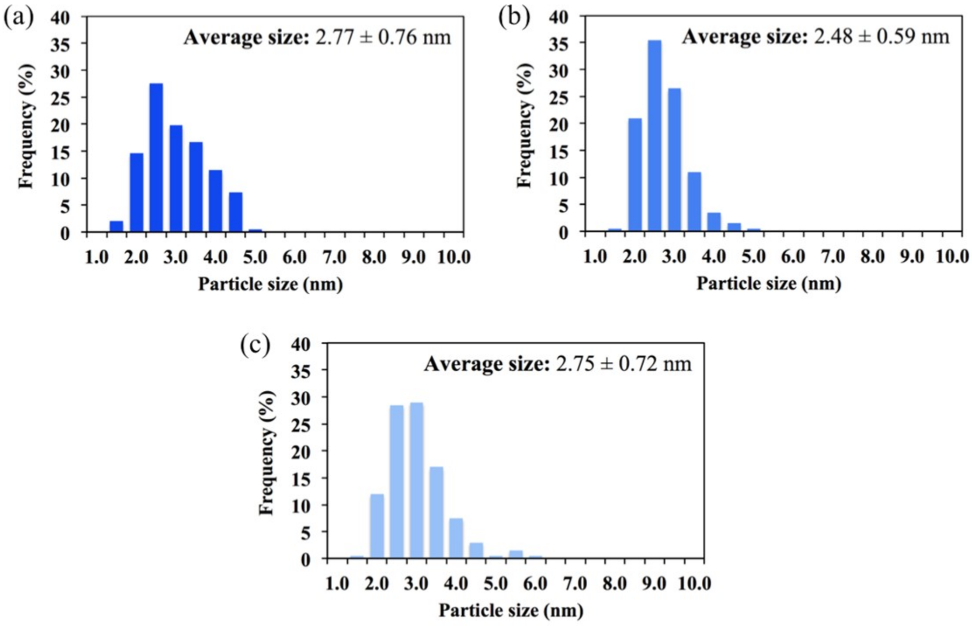

Fig. S16 Pt particle size distribution (<10 nm) and corresponding average sizes over Pt/$Ti_3C_2(OH)_x$ with increasing theoretical Pt contents of (a) 20 wt.%, (b) 30 wt.%, and (c) 40 wt.%.

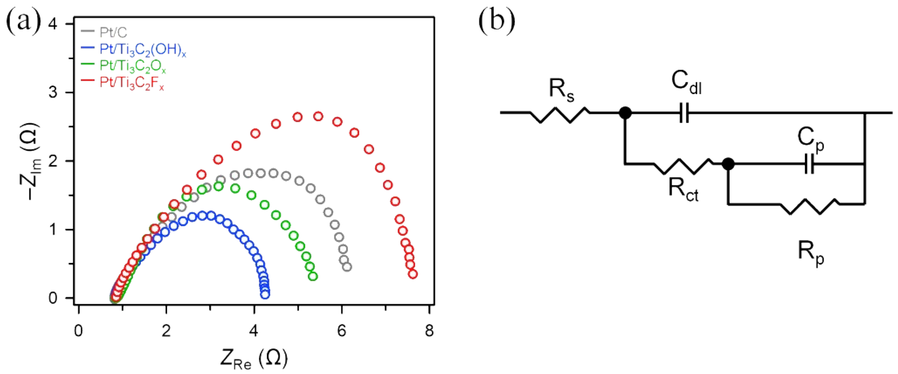

Fig. S17 (a) Nyquist plots of Pt/$Ti_3C_2T_x$ samples (Pt/$Ti_3C_2(OH)_x$, Pt/$Ti_3C_2O_x$, and Pt/$Ti_3C_2F_x$) and Pt/C catalysts measured in 1 M KOH solution. (b) Equivalent circuit fitting the EIS data.

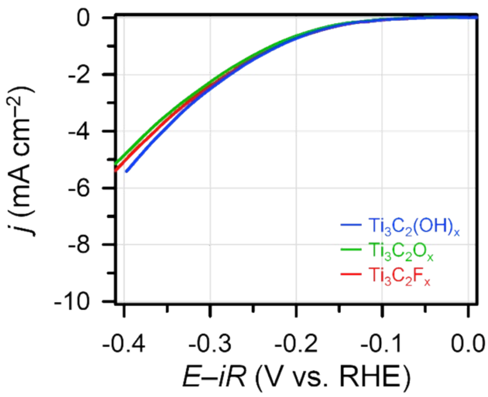

Fig. S18 HER LSV curves of $Ti_3C_2T_x$ samples measured in 1 M KOH solution.

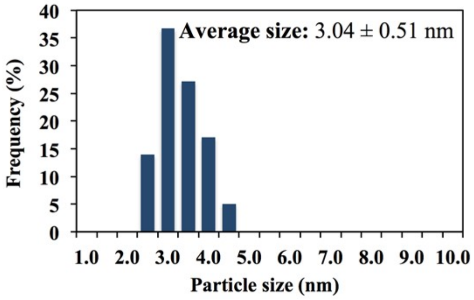

Fig. S19 Pt particle size distribution (<10 nm) and corresponding average sizes over Pt/$Ti_3C_2(OH)_x$ after catalytic stability assessment (50 h).

Table S4 Comparison of the alkaline HER activity of the catalysts presented in this work with that of previously reported Pt-based catalysts.

Catalyst	Pt loading [μg_{Pt} cm^{-2}]	Alkaline electrolyte	η_{-10}^{a} [mV]	Tafel slope [mV dec^{-1}]	Stability (h)^{b}	Ref.
$Pt/Ti_3C_2(OH)_x$	10	1 M KOH	**58**	**30**	**200**	This work
Reference: Pt/C	10	1 M KOH	87	61	-	This work
PtNi frames/$Ni(OH)_2$	14	0.1 M KOH	89	-	30	[S8]
$Ni(OH)_2$/Pt island/Pt(111)	-	0.1 M KOH	138	-	-	[S8]
$Ni(OH)_2$/Pt/C	60	0.1 M KOH	90	-	-	[S8]
Pt(111)-$Ni(OH)_2$	-	0.1 M KOH	110	-	Surface analysis: 50 cycles (–0.1 to 0.35 V_{RHE})	[S9]
$Ni(OH)_2$-modified Pt surface	-	0.1 M KOH	75	-	-	[S10]
Pt(111) with Co^{2+}	-	0.1 M KOH	200	-	-	[S11]
Pt/Cu nanowire	100	0.1 M KOH	13 @ η_{-5}	-	500 cycles (0.05 to 1.2 V_{RHE})	[S12]
Rh/Pt(poly)	-	0.1 M NaOH	93	52	-	[S13]
Pt_3Ni nanoframe/C	-	1 M KOH	88	-	10000 cycles (0.6 to 1.0 V_{RHE})	[S14]
$Ni(OH)_2$-Pt/C hybrid	1.13	1 M KOH	157	-	-	[S15]
Pt NWs/SL-$Ni(OH)_2$	16	1 M KOH	100	-	~ 1	[S16]
Ru@Pt (1 ML)	200	1 M KOH	5	-	-	[S17]
Pt_3Ni_4 NWs/C-air	15.3	1 M KOH	50	-	3	[S18]
Pt NPs/$Co(OH)_2$	390	1 M KOH	32	70	20	[S19]
Pt NPs/Ni_3N	2000	1 M KOH	50	36.5	60	[S20]
Pt–Ni/NiS/C	15.3	1 M KOH	42	-	5	[S21]
PtNi-O nanostructure	5.1	1 M KOH	39.8	78.8	10	[S22]
Pt–M NW	15.3	1 M KOH	20	79.2	-	[S23]
Pt/MMC	14	1 M KOH	45	30	1000 cycles (0.1 to –0.3 V)	[S24]

$^{a.}$ overpotential at –10 mA cm^{-2}. $^{b.}$ maximum indicated in each report.

Table S5 Comparison of the HER activity of the $Pt/Ti_3C_2(OH)_x$ catalyst reported in this work with that of previously reported $Pt/Ti_3C_2T_x$-based catalysts and other representative MXene-based systems.

Catalyst	**Pt loading [μg_{Pt} cm^{-2}]**	**Electrolyte**	**η_{-10}[a] [mV]**	**Tafel slope [mV dec^{-1}]**	**Stability (h)[b]**	**Ref.**
$Pt/Ti_3C_2(OH)_x$	10	1 M KOH	**58**	**30**	**200**	This work
Reference: Pt/C	10	1 M KOH	87	61	-	This work
$Pt/Ti_3C_2X_x$ (sub-nanometer Pt clusters)	7.4	0.5 M H_2SO_4	34	29.7	~ 3	[S25]
$Pt/Ti_3C_2X_x$ (Pt loading: ALD)	10	0.5 M H_2SO_4	67.8	69.8	20	[S26]
$Pt/Ti_3C_2X_x$	4.6	0.5 M H_2SO_4	55	65	20	[S27]
$Pt/Ti_3C_2X_x$ (multilevel hollow structures)	4.8	0.5 M H_2SO_4	13	24.2	400	[S28]
	4.8	1 M KOH	27	41	350	[S28]
Reference: Pt/C	-	1 M KOH	53	49	-	[S28]
$Ti_3C_2X_x$@Pt/SWCNTs	-	0.5 M H_2SO_4	62	78	800 (5 pieces)	[S29]
$Pt/Ti_3C_2X_x$ (with *in situ* formed Pt_3Ti)	20	0.1 M $HClO_4$	32.7	32.3	2000 cycles (–0.2 to 0.1 V_{RHE})	[S30]
$Mo_2TiC_2T_x$-single atom Pt	11	0.5 M H_2SO_4	30	30	100	[S31]
$Co_xMo_{2-x}C/Ti_3C_2X_x$/N-doped Carbon	-	1.0 M KOH	75	43	100	[S32]

[a] overpotential at –10 mA cm^{-2}. [b] maximum indicated in each report.

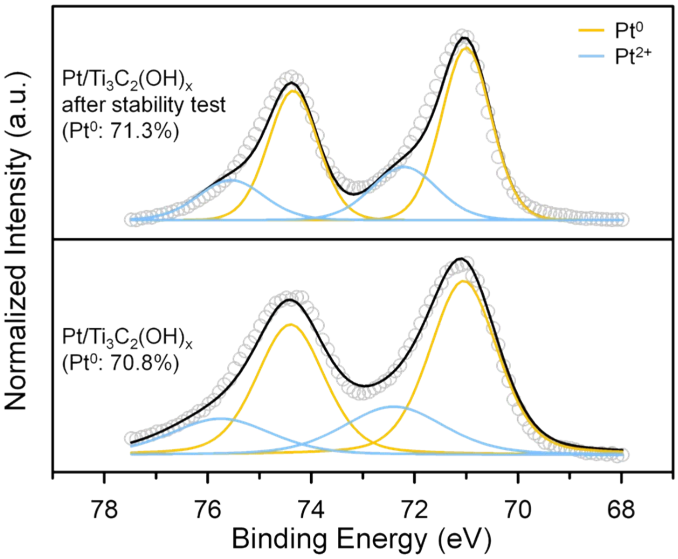

Fig. S20 Pt 4f XPS spectra for $Pt/Ti_3C_2(OH)_x$ before and after the HER stability test.

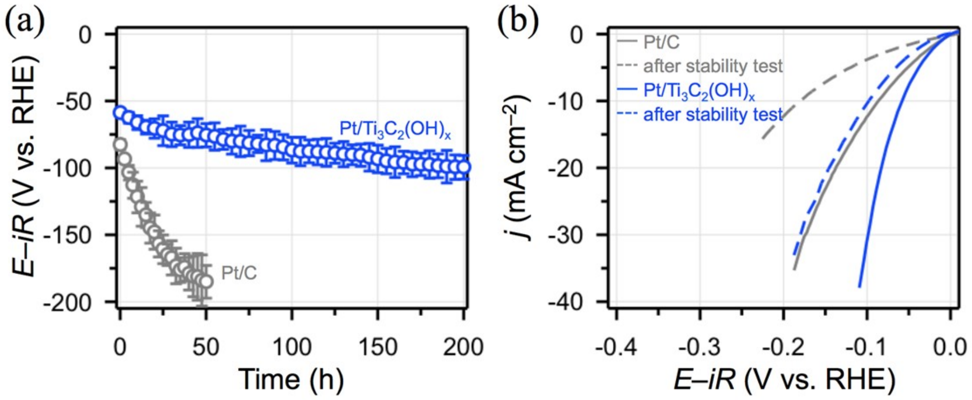

Fig. S21 (a) Stability measurements of $Pt/Ti_3C_2(OH)_x$ and Pt/C catalysts performed by chronopotentiometry at –10 mA cm^{-2} for 200 h. (b) LSV curves before and after the HER stability test of $Pt/Ti_3C_2(OH)_x$ (200 h) and Pt/C (50 h) catalysts.

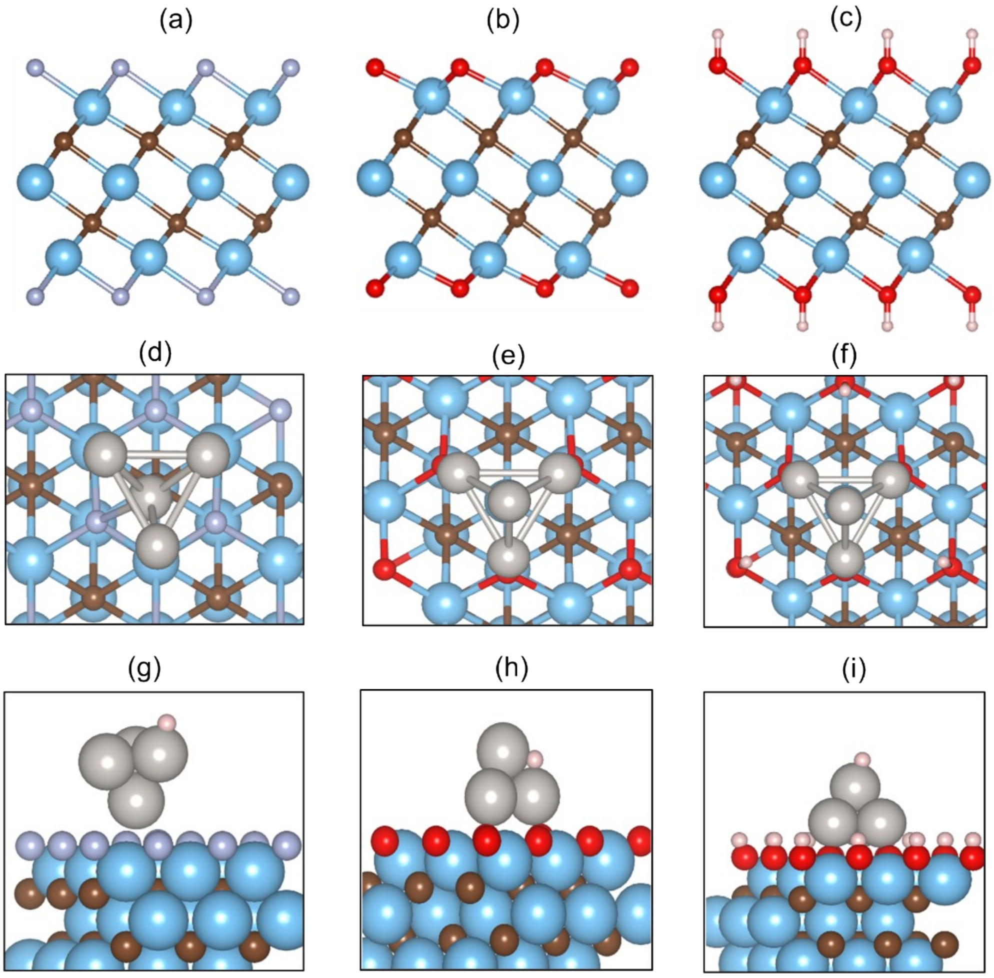

Fig. S22 Optimized structures of (a) $Ti_3C_2F_2$, (b) $Ti_3C_2O_2$, (c) $Ti_3C_2(OH)_2$, (d) Pt/ $Ti_3C_2F_2$, (e) Pt/ $Ti_3C_2O_2$, (f) Pt/$Ti_3C_2(OH)_2$, H adsorbed structure of (g) Pt/$Ti_3C_2F_2$, (h) Pt/$Ti_3C_2O_2$, (i) Pt/$Ti_3C_2(OH)_2$ (blue: Ti, brown: C, purple: F, red: O, pink: H).

References

S1 G. Kresse and J. Furthmüller, *Phys. Rev. B,* 1996, **54**, 11169.

S2 P. E. Blöchl, *Phys. Rev. B,* 1994, **50**, 17953.

S3 J. P. Perdew and A. Zunger, *Phys. Rev. B: Condens. Matter Mater. Phys.,* 1981, **23**, 5048–5079.

S4 J. P. Perdew, K. Burke and M. Ernzerhof, *Phys. Rev. Lett.,* 1996, **77**, 3865–3868.

S5 H. J. Monkhorst and J. D. Pack, *Phys. Rev. B: Solid State*, 1976, **13**, 5188–5192.

S6 J. K. Nørskov, J. Rossmeisl, A. Logadottir, L. Lindqvist, J. R. Kitchin, T. Bligaard and H. Jónsson, *J. Phys. Chem. B.,* 2004, **108**, 17886.

S7 NIST Standard Reference Database, https://webbook.nist.gov/chemistry/

S8 R. Subbaraman, D. Tripkovic, D. Strmcnik, K.-C. Chang, M. Uchimura, A. P. Paulikas, V. Stamenkovic and N. M. Markovic, *Science,* 2011, **334**, 1256–1260.

S9 R. Subbaraman, D. Tripkovic, K.-C. Chang, D. Strmcnik, A. P. Paulikas, P. Hirunsit, M. Chan, J. Greeley, V. Stamenkovic and N. M. Markovic, *Nat. Mater.,* 2012, **11**, 550–557.

S10 N. Danilovic, R. Subbaraman, D. Strmcnik, K.-C. Chang, A. P. Paulikas, V. R. Stamenkovic and N. M. Markovic, *Angew. Chem., Int. Ed.,* 2012, **124**, 12663–12666.

S11 R. Subbaraman, N. Danilovic, P. P. Lopes, D. Tripkovic, D. Strmcnik, V. R. Stamenkovic and N. M. Markovic, *J. Phys. Chem. C,* 2012, **116**, 22231–22237.

S12 S. M. Alia, B. S. Pivovar and Y. Yan, *J. Am. Chem. Soc.,* 2013, **135**, 13473–13478.

S13 M. Smiljanic, Z. Rakocevic, A. Maksic and S. Strbac, *Electrochim. Acta,* 2014, **117**, 336–343.

S14 C. Chen, Y. Kang, Z. Huo, Z. Zhu, W. Huang, H. L. Xin, J. D. Snyder, D. Li, J. A. Herron, M. Mavrikakis, M. Chi, K. L. More, Y. Li, N. M. Markovic, G. A. Somorjai, P. Yang and V. R. Stamenkovic, *Science,* 2014, **343**, 1339–1343.

S15 L. Wang, C. Lin, D. Huang, J. Chen, L. Jiang, M. Wang, L. Chi, L. Shi and J. Jin, *ACS Catal.,* 2015, **5**, 3801–3806.

S16 H. Yin, S. Zhao, K. Zhao, A. Muqsit, H. Tang, L. Chang, H. Zhao, Y. Gao and Z. Tang, *Nat. Commun.,* 2015, **6**, 6430.

S17 K. Elbert, J. Hu, Z. Ma, Y, Zhang, G. Chen, W. An, P. Liu, H. S. Isaacs, R. R. Adzic and J. X. Wang, *ACS Catal.,* 2015, **5**, 6764–6772.

S18 P. Wang, K. Jiang, G. Wang, J. Yao and X. Huang, *Angew. Chem., Int. Ed.,* 2016, **128**, 13051–13055.

S19 Z. Xing, C. Han, D. Wang, Q. Li and X. Yang, *ACS Catal.,* 2017, **7**, 7131–7135.

S20 Y. Wang, L. Chen, X. Yu, Y. Wang and G. Zheng, *Adv. Energy Mater.,* 2017, **7**, 1601390.

S21 P. Wang, X. Zhang, J. Zhang, S. Wan, S. Guo, G. Lu, J. Yao and X. Huang, *Nat. Commun.,* 2017, **8**, 14580.

S22 Z. Zhao, H. Liu, W. Gao, W. Xue, Z. Liu, J. Huang, X. Pan and Y. Huang, *J. Am. Chem. Soc.,* 2018, **140**, 9046–9050.

S23 Z. Liu, J. Qi, M. Liu, S. Zhang, Q. Fan, H. Liu, K. Liu, H. Zheng, Y. Yin and C. Gao, *Angew. Chem., Int. Ed.,* 2018, **57**, 11678–11682.

S24 D. S. Baek, G. W. Jung, B. Seo, J. C. Kim, H.-W. Lee, T. J. Shin, H. Y. Jeong, S. K. Kwak and S. H. Joo, *Adv. Funct. Mater.,* 2019, **29**, 1901217.

S25 Y. Wu, W. Wei, R. Yu, L. Xia, X. Hong, J. Zhu, J. Li, L. Lv, W. Chen, Y. Zhao, L. Zhou and L. Mai, *Adv. Funct. Mater.*, 2022, **32**, 2110910.

S26 X. Zhang, B. Shao, Z. Sun, Z. Gao, Y. Qin, C. Zhang, F. Cui and X. Yang, *Ind. Eng. Chem. Res.*, 2020, **59**, 1822−1828.

S27 Y. Yuan, H. Li, L. Wang, L. Zhang, D. Shi, Y. Hong and J. Sun, *ACS Sustainable Chem. Eng.*, 2019, **7**, 4266–4273.

S28 L. Xiu, W. Pei, S. Zhou, Z. Wang, P. Yang, J. Zhao and J. Qiu, *Adv. Funct. Mater.*, 2020, **30**, 1910028.

S29 C. Cui, R. Cheng, H. Zhang, C. Zhang, Y. Ma, C. Shi, B. Fan, H. Wang and X. Wang, *Adv. Funct. Mater.*, 2020, **30**, 2000693

S30 Z. Li, Z. Qi, S. Wang, T. Ma, L. Zhou, Z. Wu, X. Luan, F.-Y. Lin, M. Chen, J. T. Miller, H. Xin, W. Huang and Y. Wu, *Nano Lett.*, 2019, **19**, 5102–5108.

S31 J. Zhang, Y. Zhao, X. Guo, C. Chen, C.-L. Dong, R.-S. Liu, C.-P. Han, Y. Li, Y. Gogotsi and G. Wang, *Nature. Catal.*, 2018, **1**, 985–992.

S32 X. Wu, S. Zhou, Z. Wang, J. Liu, W. Pei, P. Yang, J. Zhao and J. Qiu, *Adv. Energy Mater.*, 2019, **9**, 1901333.